J Solid State Electrochem (2008) 12:133–141
DOI 10.1007/s10008-007-0370-9

ORIGINAL PAPER

Ball-milling processing of nanocrystalline nickel hydroxide and its effects in pasted nickel electrodes for rechargeable nickel batteries

Q. S. Song · C. H. Chiu · S. L. I. Chan

Received: 1 March 2007 / Revised: 7 May 2007 / Accepted: 29 May 2007 / Published online: 4 July 2007
© Springer-Verlag 2007

Abstract Nanocrystalline $Ni(OH)_2$ powder synthesized by a chemical precipitation method was processed using the planetary ball milling (PBM), and the physical properties of both the ball-milled and unmilled $Ni(OH)_2$ were characterized by scanning electron microscopy (SEM), specific surface area, particle size distribution, and X-ray diffraction. It was found that the PBM processing could significantly break up the agglomeration, uniformize the particle size distribution, increase the surface area, decrease the crystallite size, and reduce the crystallinity of nanocrystalline β-$Ni(OH)_2$, which were advantageous to the improvement of the electrochemical activity of $Ni(OH)_2$. The ball-milled nanocrystalline (BMN) $Ni(OH)_2$ was then used to alter the microstructure of pasted nickel electrodes and improve the distribution of the active material in the porous electrode substrate. Electrochemical performances of pasted nickel electrodes with a mixture of BMN and spherical $Ni(OH)_2$ as the active material were investigated, and were compared with those of pure spherical $Ni(OH)_2$ electrodes. Charge/discharge tests showed that BMN $Ni(OH)_2$ addition could enhance the charging efficiency, specific discharge capacity, discharge voltage, and high-rate capability of pasted nickel electrodes. This performance improvement could be attributed to a more compact electrode microstructure, better reaction reversibility, and lower electrochemical impedance, as indicated by SEM, cyclic voltammetry, and electrochemical impedance spectroscopy. Thus, it was an effective method to modify the microstructure and improve the electrochemical properties of pasted nickel electrodes by adding an appropriate amount of BMN $Ni(OH)_2$ to spherical $Ni(OH)_2$ as the active material.

Keywords Nanocrystalline nickel hydroxide · Planetary ball milling · Solid-state proton diffusion · Pasted nickel electrode · Electrode microstructure

Q. S. Song (✉)
Department of Applied Chemistry, School of Chemical Engineering and Technology, Tianjin University, Tianjin 300072, People's Republic of China
e-mail: weisu@public.tpt.tj.cn

C. H. Chiu
Department of Materials Science and Engineering, National Taiwan University, Taipei 106, Taiwan

Q. S. Song · S. L. I. Chan
School of Materials Science and Engineering, University of New South Wales, Sydney, NSW 2052, Australia

Introduction

Nickel-based rechargeable alkaline batteries (Ni/Cd, Ni/Fe, Ni/Zn, Ni/H_2, and Ni/MH) have been playing an important role in the field of electric energy storage devices for more than 100 years. Even though the further spreading of nickel-based batteries currently runs under the strong competition by the rechargeable Li-ion system which has a considerable advantage in terms of specific energy, nickel batteries still occupy a unique position within the battery industry [1–4]. Besides the very diverse applications including portable electronics, power tools, remote and stand-by power systems, satellites, and personal transportations, the nickel-based battery system appears to be the technology of choice for the emerging electric vehicles (EVs), hybrid electric vehicles (HEVs), and fuel cell electric vehicles. Among them, HEVs have been receiving much attention from both environmental and economical points of view.

The Ni/MH technology for HEVs has eventually been getting important since almost all the commercialized HEVs employ Ni/MH batteries because of their better combination of output power, capacity, life, reliability, and cost [5–7].

Nickel-based batteries are usually cathode limited, so that the capacity and cycle life of the cells are determined mainly by the properties of nickel hydroxide active materials and the corresponding electrodes. To improve the cell performance, pasted nickel electrodes made from a porous nickel-foam substrate and an active material called spherical $Ni(OH)_2$ powder have been developed [8–10]. With their high energy density and low cost relative to those of conventional sintered nickel electrodes, pasted nickel electrodes have now been widely used in commercially available Ni/MH and Ni/Zn batteries. Further enhancement is required in both specific energy and specific power of pasted nickel electrodes when they are used in batteries as the electric source for EVs, HEVs, and power tools.

As the active material of nickel electrodes, the physical and electrochemical characteristics of $Ni(OH)_2$ are the key to determine the property of the electrodes. Spherical $Ni(OH)_2$ powder with a particle size distribution from several microns to tens of microns has a high filling density and superior flow characteristics [9, 11], which are beneficial to the increase in the amount of the active material loaded in the electrode substrate and the improvement of energy density of nickel electrodes. However, the electrochemical properties of spherical $Ni(OH)_2$ are inferior, e.g., the charging efficiency, active material utilization, electronic conductivity, and proton diffusion ability are quite low [12, 13]. So considerable interest has centered on the improvement of the electrochemical activity of $Ni(OH)_2$. Besides the composition and doping level (cobalt, zinc, etc.), some physical and structural properties strongly influence the electrochemical performance of nickel hydroxide powder materials, such as the morphology, particle size and size distribution, degree of porosity, surface area, structural defects, crystal form, and crystallite size [14–18]. In particular, the crystallite size and crystallinity have been proven to be in strong correlation to the electrochemical activity of nickel hydroxide active materials. Studies [4, 9, 19–21] showed that $Ni(OH)_2$ with fine crystallite size and reduced crystallinity possessed a high chemical proton diffusion coefficient and an increased nickel utilization, giving an excellent charge/discharge cycling behavior. This has also led to the development of nanostructured nickel hydroxide as a promising electrode material for high-performance nickel-based batteries [22–25].

Another key component of pasted nickel electrodes is the highly porous nickel-foam, the substrate of the electrodes. It has a typical volumetric porosity of 95–97% and a pore size of 400–700 μm [26]. As compared with the sintered nickel substrate, the higher porosity and larger pore size of nickel-foam allow for easy access of the $Ni(OH)_2$ slurry in the pasting process and result in high filling density of the active material, but they also increase the contact resistance both between the substrate and $Ni(OH)_2$ particles and among the $Ni(OH)_2$ particles themselves. Thus, the power capability of pasted nickel electrodes is usually inferior to that of sintered nickel electrodes. To enhance the conductivity and high-rate capability of pasted nickel electrodes, one common practice in the battery industry is to use a substantial amount of conductive additives such as Co or Co compounds [8, 27–30], a major cost factor in the manufacture of pasted electrodes. Another effective approach is to modify the microstructure of the electrodes and improve the distribution or homogeneity of the active material and additives in the nickel-foam substrate, e.g., reducing the final electrode thickness and/or enhancing the packing efficiency of $Ni(OH)_2$ particles in the porous electrode substrate [31, 32].

Mechanochemical processing of materials by ball milling is an attractive technique for preparing novel materials, e.g., amorphous and nanocrystalline materials [33]. In comparison with other methods for the processing of materials, the ball-milling technique is advantageous because it is based on simple processes and shows high efficiency, low energy consumption, and low cost. This technique has been widely applied to prepare hydrogen storage alloys for Ni/MH batteries and electrode materials for Li-ion batteries [34–36]. In the literature, a method of high-energy ball milling (HEBM) was used to modify the structure and electrochemical performance of $Ni(OH)_2$, and the ball-milled $Ni(OH)_2$ was directly utilized as the active material of Ni/MH batteries. The experimental results showed that HEBM was an effective method to improve the discharge properties of β-$Ni(OH)_2$ such as specific discharge capacity, discharge potential, and cycle performance, while the performance of α-$Ni(OH)_2$ was greatly reduced by HEBM processing [37]. Casas-Cabanas et al. [38] employed the low-energy milling treatment to improve the material distribution and homogeneity of the mixture of β-$Ni(OH)_2$ and graphite, which was used as the active material for a pocket-plate electrode. They found that the capacity of the $Ni(OH)_2$ sample with added graphite was increased with the increase in milling time.

In theory, the size of tetrahedral interstices in pasted nickel electrodes, which are formed by the close-stacking of spherical $Ni(OH)_2$ with a particle size of 9 μm, is around 2 μm [39]. Thus, if small $Ni(OH)_2$ particles with the size of ~2 μm are used to fill these interstitial voids, the packing efficiency of $Ni(OH)_2$ active materials in the electrode could be much improved. This will subsequently result in an enhancement of the material utilization and high-rate capability of the electrode. In our previous work [40, 41], the normal ball milling (NBM) was used to

modify the commercial spherical $Ni(OH)_2$ powder, and it was found that the average particle size of spherical Ni $(OH)_2$ was decreased from 8.839 to 1.926 μm by NBM with a milling time of 120 h. From the industrial point of view, it is highly desirable that the milling time can be significantly reduced and the treatment efficiency can be much improved. This might be realized by using a higher energy milling technique, such as the planetary ball milling (PBM). In this paper, nanocrystalline $Ni(OH)_2$ powder synthesized by a chemical precipitation method was processed using PBM to break up the agglomeration and further improve the electrochemical activity. The physical and structural features of the ball-milled nanocrystalline (BMN) $Ni(OH)_2$ were characterized and correlated to the electrochemical activity of $Ni(OH)_2$. The BMN $Ni(OH)_2$ with a particle size of ~2 μm was then adopted to alter the microstructure of pasted nickel electrodes and improve the distribution and packing efficiency of the active material in the porous electrode substrate. The electrochemical properties of pasted nickel electrodes with an addition of BMN $Ni(OH)_2$ to spherical $Ni(OH)_2$ as the active material were investigated by charge/discharge tests, cyclic voltammetry (CV), and electrochemical impedance spectroscopy (EIS). The mechanism for the effect of BMN $Ni(OH)_2$ in pasted nickel electrodes was also examined. We reported that it was an effective method to modify the microstructure and improve the electrochemical performance of pasted nickel electrodes by adding an appropriate amount of BMN $Ni(OH)_2$ to spherical $Ni(OH)_2$ as the active material.

Experimental

PBM processing and physical characterization of nickel hydroxide powders

Nanocrystalline nickel hydroxide powder was synthesized by a chemical precipitation method as described in the literature [13]. The synthesized powder material was subsequently subjected to a milling processing in a planetary ball mill. The ball to powder mass ratio was 8:1 and the duration of milling was scheduled between 4 to 48 h. The crystallographic structure of $Ni(OH)_2$ powders was characterized by X-ray diffraction (XRD) with a Rigaku diffractometer using Cu Kα radiation (λ=1.542 Å). Scanning electron microscopy (SEM) observation was performed using a LEO 1530 microscope. The specific surface area was evaluated by the Brunauer-Emmett-Teller (BET) nitrogen adsorption method using a CHEMBET-3000 surface area analyzer. The particle size distribution of the powders was obtained using a Mastersizer 2000 particle size analyzer. The properties of the commercial spherical $Ni(OH)_2$ powder (from NEXcell Battery Co., Ltd) were also examined and compared with those of the nanocrystalline $Ni(OH)_2$ powders before and after PBM processing.

Preparation and electrochemical testing of pasted nickel electrodes

Pasted nickel electrodes with an addition of BMN $Ni(OH)_2$ were prepared as follows: 8 wt% nanocrystalline $Ni(OH)_2$ powder ball-milled with 48 h was mixed thoroughly with 92 wt% spherical $Ni(OH)_2$ powder as the active material, 10 wt% nickel and 5 wt% CoO powders were used as conductors, and 3 wt% suspension containing 60 wt% polytetrafluoroethylene (PTFE) and 1.5 wt% carboxymethyl cellulose (CMC) was added to the mixed powders as a binder. The mixture was then blended to obtain a paste. The resulting paste was incorporated into a 2×2-cm nickel-foam substrate, to which a nickel ribbon was spot-welded as a current collector. Subsequently, the pasted electrodes were dried at 80 °C for 2–3 h and pressed at 175 MPa to assure good electrical contact between the substrate and the active material. The content of $Ni(OH)_2$ active material in the resultant electrodes was determined through the weight ratio of different electrode components. For comparison, the nickel electrodes without the addition of BMN $Ni(OH)_2$ were also prepared using pure spherical $Ni(OH)_2$ powder as the active material. The morphology and microstructure of the as-prepared nickel electrodes were examined by SEM using a LEO 1530 microscope.

Charge/discharge studies were conducted in a test cell, including the as-prepared nickel electrodes as the cathode and a hydrogen-storage alloy [$Mm(Ni–Co–Mn–Al)_5$] electrode as the anode. Polypropylene was used as the separator between the cathode and anode. The electrolyte solution consisted of 6 M KOH + 1 wt% LiOH. The cell capacity was cathodically limited. The test cells were charged at a rate of 0.2 C for 6 h, and discharged at the same rate down to a cut-off voltage of 1.0 V. After several charge/discharge cycles for cell activation, the discharge characteristics at various rates (0.2, 0.5, 1.0, 1.5, and 2.0 C) were obtained with a fixed charge rate of 0.2 C. The tests were performed on a Kikusui PF 40W-08 cycler.

For the cyclic voltammetry (CV) and electrochemical impedance spectroscopy (EIS) measurements, a three-compartment glass cell containing 6 M KOH + 1 wt% LiOH electrolyte solution was used. The pasted nickel electrodes, which acted as the working electrode in the cell, were soaked in the electrolyte solution for 10 h before test. A hydrogen-storage alloy electrode with a capacity well in excess of the nickel electrodes was used as the counter electrode. For the reference electrode, a Hg/HgO (6 M KOH) electrode was employed, and the potential of the working electrode was monitored through a Luggin capillary with respect to the

reference electrode. The nickel electrodes were activated by charge/discharge cycling before the experiments, and were then cycled several times by CV to obtain a stable profile. The voltammograms were recorded at a sweep rate of 0.1 mV s^{-1}, with a sweep potential range of 0.1 to 0.7 V vs Hg/HgO. For the EIS studies, the impedance spectra were recorded at a 5-mV amplitude of perturbation, with a sweep frequency range of 20 kHz to 1 mHz. The tests were performed using an Autolab PGSTAT30 system. All the electrochemical measurements were carried out at ambient temperature.

Results and discussion

SEM and BET analyses

Figure 1 shows the scanning electron micrographs at a high magnification for the commercial spherical $Ni(OH)_2$ (sample A), as-synthesized nanocrystalline $Ni(OH)_2$ (sample B), and nanocrystalline $Ni(OH)_2$ ball-milled with 48 h (sample C), respectively. It can be seen that $Ni(OH)_2$ particles consist of many tiny crystals. Sample A is made up of stacks of thin plate-like crystals, and the surface porosity of the powder is low due to the relatively close stacking of the crystals. While sample B possesses a unique surface texture with ultrathin flake-like nanocrystals and a high porosity, suggesting a high specific surface area for the electrochemical redox reaction. After PBM for 48 h, sample C has a rougher surface with much more flake-like nanocrystals projecting from the powder, which can further increase the surface area. From the BET measurement, the specific surface areas of $Ni(OH)_2$ samples A, B, and C are 10, 30, and 42 m^2 g^{-1}, respectively, indicating the highest surface area of sample C. For the active material of nickel electrodes, a high specific surface area can provide a high density of active sites and promote intimate interaction of the active material with the surrounding electrolyte [13, 14]. Therefore, better electrochemical reactivity of the BMN $Ni(OH)_2$ powder will be facilitated by the high surface area.

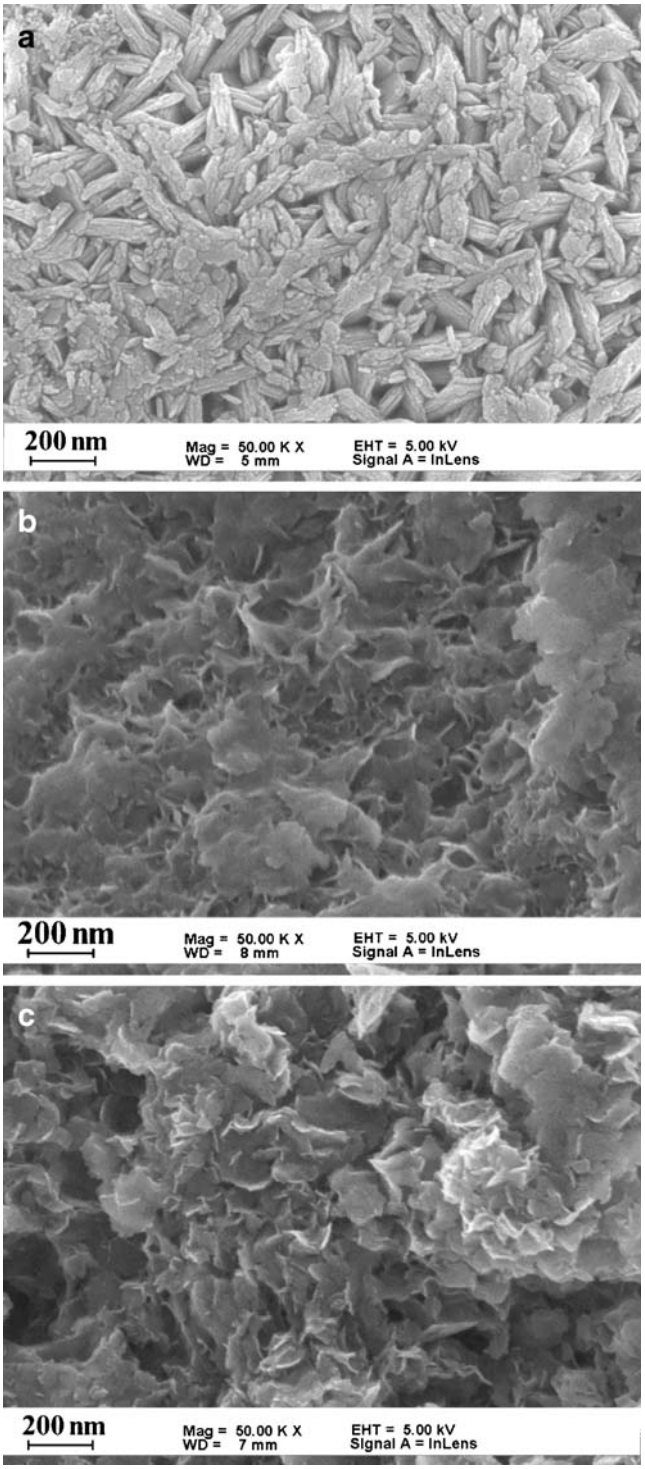

Fig. 1 SEM photographs at a high magnification for (**a**) commercial spherical $Ni(OH)_2$, (**b**) as-synthesized nanocrystalline $Ni(OH)_2$, and (**c**) nanocrystalline $Ni(OH)_2$ ball-milled with 48 h

Particle size distribution

To investigate the effect of the PBM processing on the agglomerate size of nanocrystalline $Ni(OH)_2$ powders, the particle size distribution of the powders was measured and the average particle size (d_{50}) was obtained. Figure 2 shows the particle size distribution at various milling times for nanocrystalline $Ni(OH)_2$ powders. It is noted that the average particle size is markedly decreased from 13.13 to 3.43 μm during 12 h of the milling time, and is further decreased to 1.97 μm by PBM when the milling time is reached at 48 h. Meanwhile, the as-synthesized nanocrystalline $Ni(OH)_2$ possesses a relatively wide range of size distribution with a small distribution curve around 2 μm, which gets less obvious at 12 h of the milling time and finally disappears after PBM for 48 h. This implies that the size of both the large agglomerates (~13 μm) and the small particles (~2 μm) is reduced during PBM and the size

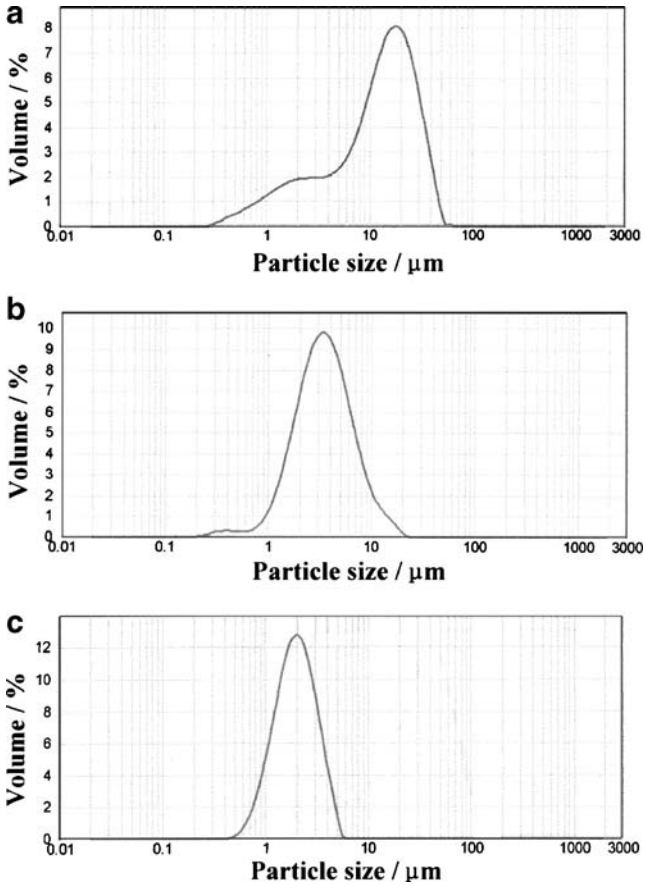

Fig. 2 Particle size distribution at various milling times for nanocrystalline $Ni(OH)_2$ powders: (**a**) before ball milling, d_{50}=13.13 μm; (**b**) ball-milled with 12 h, d_{50}=3.43 μm; and (**c**) ball-milled with 48 h, d_{50}=1.97 μm

distribution becomes much more uniform with an increase in the milling time. In comparison with 120 h of the milling time for the normal ball milling (NBM) [40, 41], the milling time is much reduced for PBM to obtain the similar results. Thus, PBM is a more effective process to break up the agglomeration and enhance the homogeneity of the size distribution of nanocrystalline $Ni(OH)_2$ powder materials.

XRD patterns

XRD patterns of $Ni(OH)_2$ samples A, B, and C are presented in Fig. 3a–c, respectively. The characteristic diffraction peaks at (001)($d_{4.60}$), (100)($d_{2.70}$), (101)($d_{2.34}$), (102)($d_{1.76}$), (110)($d_{1.56}$), and (111)($d_{1.48}$) show that all these $Ni(OH)_2$ samples have a β-type crystal structure. β-$Ni(OH)_2$ crystallizes with a hexagonal brucite structure. The intersheet distance c of the layered structure of Ni $(OH)_2$ is represented by the d_{001} value. The d_{100} or d_{110} value corresponds to the Ni–Ni distance a in the layers of $Ni(OH)_2$, where $a=[2/3^{1/2}]d_{100}$ or $2d_{110}$ [42, 43]. The crystal parameters obtained from XRD patterns are listed in Table 1. In comparison with sample A, sample B shows

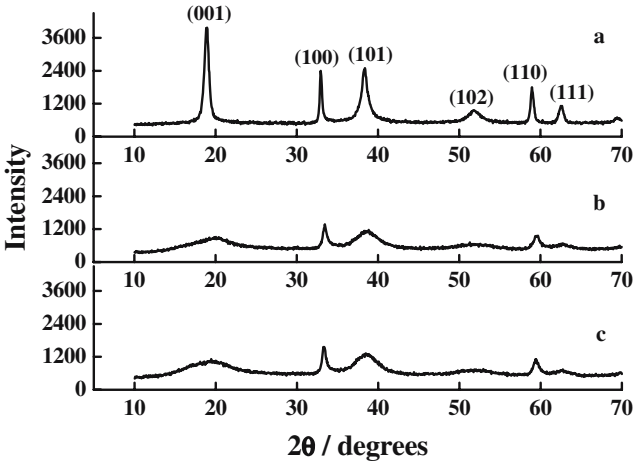

Fig. 3 XRD patterns for (**a**) commercial spherical $Ni(OH)_2$, (**b**) as-synthesized nanocrystalline $Ni(OH)_2$, and (**c**) nanocrystalline $Ni(OH)_2$ ball-milled with 48 h

some different microstructural characteristics as revealed in XRD patterns. The peaks corresponding to the (001), (101), (102), and (111) reflections in the XRD pattern of sample B are noticeably broadened as compared to those in the pattern of sample A. After PBM for 48 h, these XRD reflections for sample C are further broadened. That is, the largest full-width of half-maximum intensity (FWHM) of these peaks is obtained with the BMN $Ni(OH)_2$.

The broadening of some of the diffraction lines [e.g., (001) and (*hk*0)] is directly related to the crystallite size [19, 44]. The crystallite size D, in the direction perpendicular to various diffraction planes can be estimated from the XRD lines using the Scherrer formula:

$$D = 0.9\lambda/B\cos(\theta) \quad (1)$$

where D is the crystallite size, λ represents the X-ray wavelength, B is the FWHM, and θ is the Bragg angle. The D values of $Ni(OH)_2$ calculated from (001) and (101) XRD peaks are given in Table 1. It indicates that sample C has the smallest crystallite size among the three $Ni(OH)_2$ samples. To the best of our knowledge, the crystallite size value of sample C (BMN $Ni(OH)_2$) is also the smallest one currently available in the literature for $Ni(OH)_2$ materials.

Table 1 Experimental results of XRD analysis for $Ni(OH)_2$ powders

Parameters	Sample A	Sample B	Sample C
Crystal type	β-$Ni(OH)_2$	β-$Ni(OH)_2$	β-$Ni(OH)_2$
Crystallite size calculated from (001) peak/nm	12.29	1.72	1.46
Crystallite size calculated from (101) peak/nm	8.99	2.94	2.45
Lattice parameter c/Å	4.60	4.60	4.60
Lattice parameter a/Å	3.12	3.12	3.12

Furthermore, it has been pointed out that the abnormal broadening of the (10 *l*) reflection lines ($l \neq 0$) cannot be attributed only to the crystallite size. The existence of structural defects, such as stacking faults/growth faults and/or proton vacancies, also plays a very important role in explaining this broadening [19, 44–46]. So, besides the smallest crystallite size, sample C should also possess the most structural defects. Thus, PBM is also effective in decreasing the crystallite size and increasing the structural defects of nanocrystalline $Ni(OH)_2$ powder materials.

It is widely accepted that the nickel electrode works as an insertion electrode for protons, the redox reaction of Ni (II)/Ni(III) in alkaline media can be expressed as:

$$NiOOH + H_2O + e^- \Leftrightarrow Ni(OH)_2 + OH^- \quad (2)$$

which is believed to be a solid-state proton intercalation and deintercalation reaction [47–49]. In the charge/discharge process, the proton insertion into and desertion from the hexagonal structure of nickel hydroxide occur reversibly, and the crystal structure of nickel hydroxide is maintained. The electrochemical activity of nickel hydroxide materials can be improved by increasing the chemical proton diffusion coefficient in $Ni(OH)_2$. The small crystallite size and low crystallinity (high density of structural defects) of nickel hydroxide powder are beneficial to the acceleration of the solid-state proton diffusion in $Ni(OH)_2$ lattice, and this will diminish the concentration polarization of protons during charge/discharge, leading to a better charge/discharge cycling behavior. Therefore, the BMN $Ni(OH)_2$ is envisaged to display a superior electrochemical behavior, suggesting a promising use as a high-performance electrode material for nickel batteries.

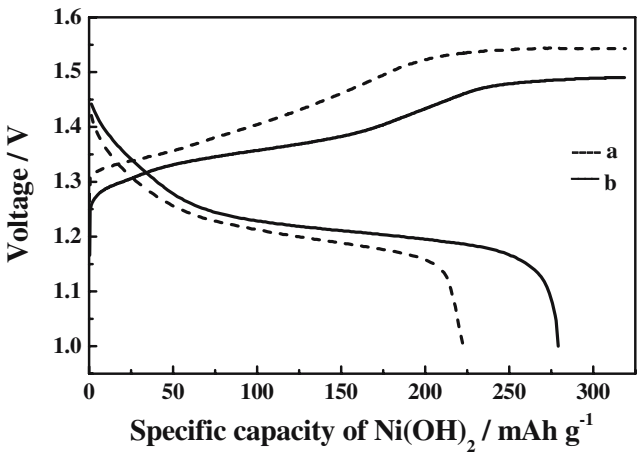

Fig. 4 Typical charge (0.2-C rate) and discharge (0.5-C rate) curves for pasted nickel electrodes: (**a**) without and (**b**) with an addition of 8 wt% BMN $Ni(OH)_2$ powder

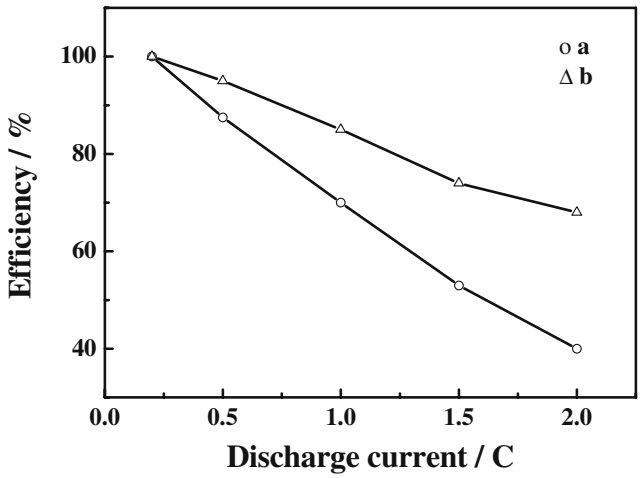

Fig. 5 High-rate discharge capability of pasted nickel electrodes: (**a**) without and (**b**) with an addition of 8 wt% BMN $Ni(OH)_2$ powder

Charge/discharge tests for pasted nickel electrodes

As discussed above, the BMN $Ni(OH)_2$ with an average particle size of ~2 μm is expected to possess a high electrochemical activity, while the commercial spherical $Ni(OH)_2$ with an average particle size of ~9 μm has been demonstrated to have a high filling density. To improve the distribution and packing efficiency of $Ni(OH)_2$ active materials in pasted nickel electrodes and simultaneously utilize the individual property advantages of these two $Ni(OH)_2$ powder materials, a mixture of the BMN and spherical $Ni(OH)_2$ powders has been used as the active material to fabricate the electrodes.

Figure 4 shows the typical charge and discharge curves for the pasted nickel electrode with pure spherical $Ni(OH)_2$ as the active material (code A) and the electrode with an addition of 8 wt% BMN $Ni(OH)_2$ to spherical $Ni(OH)_2$ (code B), the rates for the charge and discharge are 0.2 and 0.5 C, respectively. It can be seen that the charge voltage of electrode B is lower than that of electrode A, which implies that the former has better chargeability and lower intrinsic resistance. The specific discharge capacity of electrode B is larger than that of electrode A, and the discharge voltage of electrode B is also higher than electrode A. Figure 5 gives the high-rate discharge capability of electrodes A and B, in which the efficiency denotes the ratio of the capacity at various rates to the capacity at the 0.2-C rate. The experimental results show that BMN $Ni(OH)_2$ addition can considerably enhance the high-rate discharge efficiency of pasted nickel electrodes, and the effect becomes more remarkable with an increase in the discharge rate. This indicates that the addition of BMN $Ni(OH)_2$ to spherical $Ni(OH)_2$ not only can increase the discharge capacity and utilization of nickel hydroxide active material, but can also improve the discharge voltage and high-rate capability of nickel electrodes. Given these findings, it can be concluded

that the nickel electrode with added BMN $Ni(OH)_2$ experiences less polarization during the charge/discharge process as compared with the electrode without BMN $Ni(OH)_2$. This conclusion is corroborated by CV and EIS studies.

CV and EIS measurements of pasted nickel electrodes

The cyclic voltammograms of pasted nickel electrodes A and B are shown in Fig. 6. For both electrodes, one anodic nickel hydroxide ($Ni(OH)_2$) oxidation peak, appearing at about 500 to 550 mV, is recorded before oxygen evolution. Similarly, one cathodic oxyhydroxide (NiOOH) reduction peak at about 300 to 320 mV is observed on the reverse sweep. To compare the CV characteristics of electrodes A and B, the results of CV measurements are tabulated in Table 2.

The average of the cathodic and anodic peak potentials (E_{rev}) can be taken as an estimate of the reversible potential for nickel electrodes, and the difference in the anodic and cathodic peak potentials ($\Delta E_{a,c}$) is a measure of the reversibility of the redox reaction [14]. The experimental data in Table 2 show that the redox reactions are somewhat quasireversible for electrodes A and B, as indicated by the relatively large $\Delta E_{a,c}$. However, the $\Delta E_{a,c}$ of electrode B is smaller than that of electrode A, which suggests that electrode B with added BMN $Ni(OH)_2$ has better reaction reversibility. Furthermore, electrode B also has a slightly more cathodic reversible potential.

As shown in Table 2, both the anodic and cathodic peak current densities for electrode B are higher than those of electrode A at the same potential sweep rate. This indicates that more active materials can be utilized on the surface of electrode B during the charge/discharge process, suggesting that the nickel electrode with added BMN $Ni(OH)_2$ has better electrochemical reactivity and higher active material utilization. Thus, a higher charging efficiency and a greater discharge capacity can be obtained with electrode B.

Table 2 Experimental results of CV measurements for pasted nickel electrodes

Parameters	Electrode A	Electrode B
Anodic peak potential E_a/mV	558	516
Cathodic peak potential E_c/mV	301	318
Average potential E_{rev}/mV	430	417
Peak separation $\Delta E_{a,c}$/mV	257	198
Anodic peak current I_a/mA cm^{-2}	398	447
Cathodic peak current I_c/mA cm^{-2}	252	306

In comparison with those of electrode A, the anodic peak potential of electrode B is obviously shifted to a more cathodic value, while the cathodic peak potential is shifted to a more anodic value. As indicated by the above charge/discharge studies, electrode B has a lower charge voltage and a higher discharge voltage as compared with electrode A. Thus, the observation for the oxidation and reduction potentials from CV is consistent with the experimental results of the charge and discharge voltages, implying again that electrode B has a smaller polarization during the charge/discharge process.

Figure 7 shows the electrochemical impedance spectra for electrodes A and B. The impedance spectra of these two electrodes display a depressed semicircle resulting from the charge transfer resistance in the high-frequency region, and a slope related to the Warburg impedance appearing in the low-frequency region [50, 51]. A fitting calculation was performed on the spectra using the electrical equivalent circuit which consisted of the elements of the electrolyte resistance (R_s), the charge transfer resistance (R_{ct}), the double-layer capacitance (C_d), and the Warburg impedance

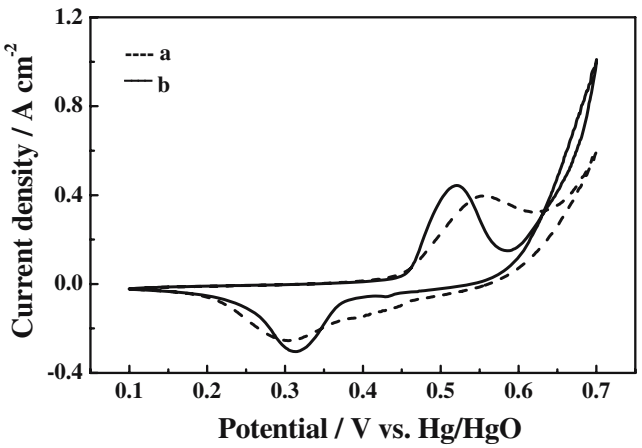

Fig. 6 Cyclic voltammograms for pasted nickel electrodes: (**a**) without and (**b**) with an addition of 8 wt% BMN $Ni(OH)_2$ powder

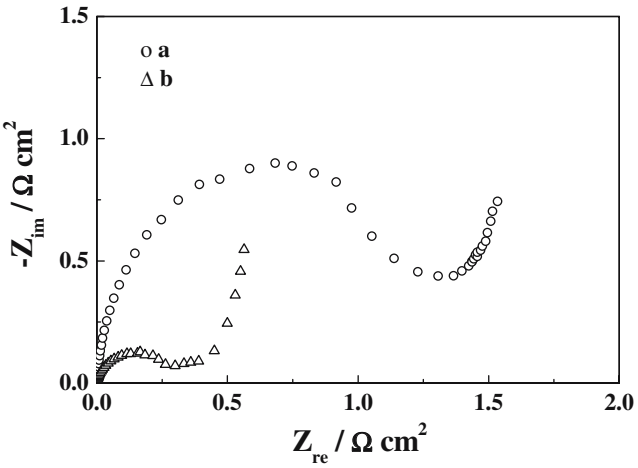

Fig. 7 Electrochemical impedance spectra of pasted nickel electrodes: (**a**) without and (**b**) with an addition of 8 wt% BMN $Ni(OH)_2$ powder

(W_0). The simulated values of R_{ct} for electrodes A and B were found to be 1.12 and 0.31 Ω cm^2, respectively. It is evident that the charge transfer resistance of electrode B with added BMN $Ni(OH)_2$ is much smaller than that of electrode A without BMN $Ni(OH)_2$. This implies that the electrochemical reaction on electrode B proceeds more easily than that on electrode A.

SEM analysis for pasted nickel electrodes

To investigate the effect of BMN $Ni(OH)_2$ addition on the morphology and microstructure of pasted nickel electrodes, SEM micrographs for the as-prepared electrodes A and B before charge/discharge cycling are presented in Fig. 8. It is noted that there are many large pores with a size of several microns between the spherical $Ni(OH)_2$ particles among electrode A, which will cause a high resistance for the transfer of electrons and ions in the electrode during the charge/discharge process. For electrode B with added BMN $Ni(OH)_2$, small ball-milled particles are embedded between the larger $Ni(OH)_2$ spheres, indicating a more compact electrode microstructure. So the interconnectivity of spherical $Ni(OH)_2$ particles among electrode B is much enhanced through the linkage of BMN $Ni(OH)_2$ particles, which will result in a shorter current conducting pathway in the active material and a better degree of contact between the nickel electrode and the electrolyte. Thus, this kind of electrode microstructure can facilitate the rapid movement of both electrons and ions in the electrode and lower the internal resistance of the electrode. Meanwhile, with high electrochemical activity the BMN $Ni(OH)_2$ particles themselves can also participate in the charge/discharge reaction and make a contribution to the capacity of the electrode. Accordingly, BMN $Ni(OH)_2$ addition can reduce the electrochemical reaction impedance and enhance the charge/discharge cycling properties of pasted nickel electrodes.

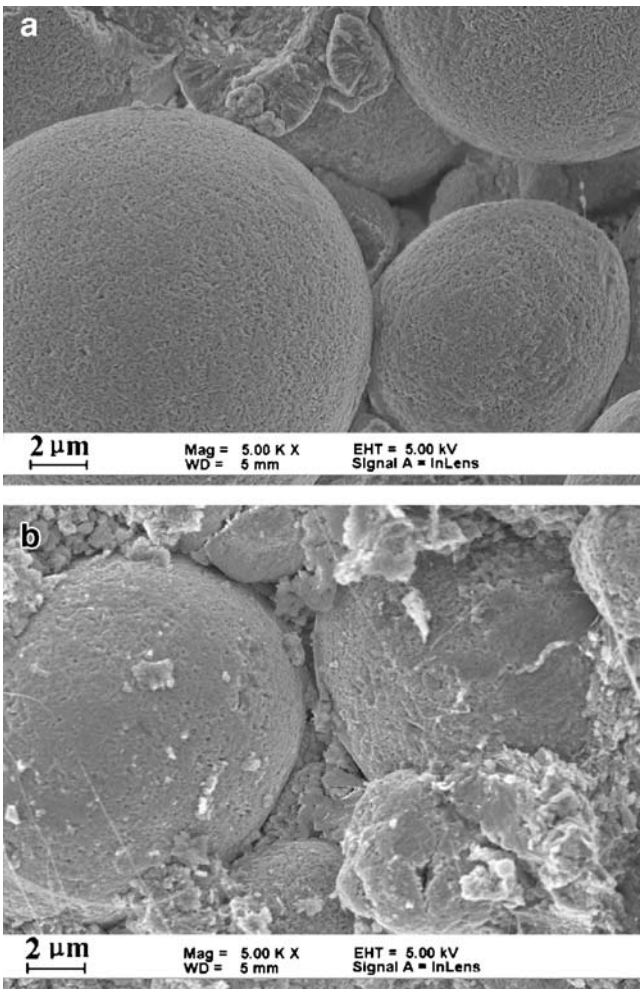

Fig. 8 SEM photographs for as-prepared pasted nickel electrodes: (**a**) without and (**b**) with an addition of 8 wt% BMN $Ni(OH)_2$ powder

Conclusions

The planetary ball milling (PBM) has been used to process the nanocrystalline nickel hydroxide powder, which was synthesized by a chemical precipitation method. It is found that the PBM processing can significantly break up the agglomeration, uniformize the particle size distribution, and increase the surface area of nanocrystalline β-$Ni(OH)_2$ particles. Structural characterization shows that PBM is also effective in reducing the crystallite size and increasing the structural defects of nanocrystalline β-$Ni(OH)_2$. These changes in physical and structural characteristics induced by PBM are advantageous to the improvement of the electrochemical activity of nanocrystalline $Ni(OH)_2$ powder materials.

Electrochemical measurements reveal that the pasted nickel electrode with a mixture of the ball-milled nanocrystalline (BMN) $Ni(OH)_2$ and commercial spherical $Ni(OH)_2$ as the active material exhibits superior charge/discharge performances in comparison with those of the electrode prepared with pure spherical $Ni(OH)_2$. That is, a greater discharge capacity, a higher charging efficiency, better high-rate capability, and a higher discharge voltage can be obtained for the nickel electrode with the addition of 8 wt% BMN $Ni(OH)_2$. SEM examination shows that the homogeneous embedment of small BMN $Ni(OH)_2$ particles between the larger $Ni(OH)_2$ spheres forms a more compact electrode microstructure, which results in better interconnectivity of spherical $Ni(OH)_2$ particles and a shorter current conducting pathway in the electrode. Furthermore, compared with the pure spherical $Ni(OH)_2$ electrode, the nickel electrode with added BMN $Ni(OH)_2$ possesses better reaction reversibility and lower electrochemical impedance, as indicated by CV and EIS studies. Therefore, it is a promising method to modify the microstructure

and improve the electrochemical performance of pasted nickel electrodes by adding an appropriate amount of BMN $Ni(OH)_2$ to spherical $Ni(OH)_2$ as the active material.

Acknowledgements This work was supported by the Tianjin Municipal Natural Science Foundation of China (grant no. 05YFJMJC09900), and by the Project-sponsored by SRF for ROCS, the Ministry of Education of China (grant no. 2004-176).

References

1. Beck F, Ruetschi P (2000) Electrochim Acta 45:2467
2. Morioka Y, Narukawa S, Itou T (2001) J Power Sources 100:107
3. Shukla AK, Venugopalan S, Hariprakash B (2001) J Power Sources 100:125
4. Köhler U, Antonius C, Bäuerlein P (2004) J Power Sources 127:45
5. Taniguchi A, Fujioka N, Ikoma M, Ohta A (2001) J Power Sources 100:117
6. Köhler U, Kümpers J, Ullrich M (2002) J Power Sources 105:139
7. Lipp L, An W (2005) J Electrochem Soc 152:K1
8. Oshitani M, Yufu H, Takashima K, Tsuji S, Matsuma Y (1989) J Electrochem Soc 136:1590
9. Watanabe K, Kikuoka T, Kumagai N (1995) J Appl Electrochem 25:219
10. Taucher-Mautner W, Kordesch K (2004) J Power Sources 132:275
11. Munehisa I, Norikatsu A (1993) Eur Patent No EP 0523284
12. Fetcenko M (2001) Propulsion and industrial nickel-metal hydride batteries. In: Linden D, Reddy TB (eds) Handbook of batteries, 3rd edn. McGraw-Hill, pp 30.11–30.12
13. Song QS, Li YY, Chan SLI (2005) J Appl Electrochem 35:157
14. Kamath PV, Subbanna GN (1992) J Appl Electrochem 22:478
15. Audemer A, Delahaye A, Farhi R, Sac-Epee N, Tarascon JM (1997) J Electrochem Soc 144:2614
16. Gille G, Albrecht S, Meese-Marktscheffel J, Olbrich A, Schrumpf F (2002) Solid State Ionics 148:269
17. Song QS, Tang ZY, Guo HT, Chan SLI (2002) J Power Sources 112:428
18. Deabate S, Henn F (2005) Electrochim Acta 50:2823
19. Bernard MC, Cortes R, Keddam M, Takenouti H, Bernard P, Senyarich S (1996) J Power Sources 63:247
20. Delmas C, Tessier C (1997) J Mater Chem 7:1439
21. Ramesh TN, Kamath PV, Shivakumara C (2005) J Electrochem Soc 152:A806
22. Meyer M, Bée A, Talbot D, Cabuil V, Boyer JM, Répetti B, Garrigos R (2004) J Colloid Interface Sci 277:309
23. Han XJ, Xu P, Xu CQ, Zhao L, Mo ZB, Liu T (2005) Electrochim Acta 50:2763
24. He X, Li J, Cheng H, Jiang C, Wan C (2005) J Power Sources 152:285
25. Jayalakshmi M, Radhika P, Raja KP, Rao MM (2007) J Solid State Electrochem 11:165
26. Olurin OB, Wilkinson DS, Weatherly GC, Paserin V, Shu J (2003) Compos Sci Technol 63:2317
27. Pralong V, Chabre Y, Delahaye-Vidal A, Tarascon JM (2002) Solid State Ionics 147:73
28. Jayashree RS, Kamath PV (2002) J Electrochem Soc 149:A761
29. Wu JB, Tu JP, Han TA, Yang YZ, Zhang WK, Zhao XB (2006) J Power Sources 156:667
30. Tronel F, Guerlou-Demourgues L, Basterreix M, Delmas C (2006) J Power Sources 158:722
31. Fukunaga H, Kishimi M, Matsumoto N, Ozaki T, Sakai T, Tanaka T, Kishimoto T (2005) J Electrochem Soc 152:A905
32. Yang QM, Ettel VA, Babjak J, Charles DK, Mosoiu MA (2003) J Electrochem Soc 150:A543
33. Suryanarayana C (2001) Prog Mater Sci 46:1
34. Singh A, Singh BK, Davidson DJ, Srivastava ON (2004) Int J Hydrogen Energy 29:1151
35. Rongeat C, Roué L (2004) J Power Sources 132:302
36. Ning LJ, Wu YP, Fang SB, Rahm E, Holze R (2004) J Power Sources 133:229
37. Chen H, Wang JM, Pan T, Xiao HM, Zhang JQ, Cao CN (2003) Int J Hydrogen Energy 28:119
38. Casas-Cabanas M, Hernández JC, Gil V, Soria ML, Palacin MR (2004) J Power Sources 134:298
39. Heyes SJ, http://www.ncl.ox.ac.uk/icl/heyes/structure_of_solids/Strucsol.html
40. Song QS, Chiu CH, Chan SLI (2006) J Appl Electrochem 36:97
41. Song QS, Chiu CH, Chan SLI (2006) Electrochim Acta 51:6548
42. Oliva P, Leonardi J, Laurent JF, Delmas C, Braconnier JJ, Figlarz M, Fievet F, Guibert A (1982) J Power Sources 8:229
43. Faure C, Delmas C, Fouassier M (1991) J Power Sources 35:279
44. Tessier C, Haumesser PH, Bernard P, Delmas C (1999) J Electrochem Soc 146:2059
45. Deabate S, Fourgeot F, Henn F (2000) J Power Sources 87:125
46. Ramesh TN, Jayashree RS, Kamath PV (2003) Clays Clay Miner 51:570
47. Weidner JW, Timmerman P (1994) J Electrochem Soc 141:346
48. Motupally S, Streinz CC, Weidner JW (1998) J Electrochem Soc 145:29
49. Ta KP, Newman J (1998) J Electrochem Soc 145:3860
50. Reid MA, Loyselle PL (1991) J Power Sources 36:285
51. Mancier V, Métrot A, Willmann P (1996) Electrochim Acta 41:1259